

Neuromorphic weighted sum with magnetic skyrmions

Tristan da Câmara Santa Clara Gomes,^{1, a)} Yanis Sassi,¹ Dédalo Sanz-Hernández,¹ Sachin Krishnia,¹ Sophie Collin,¹ Marie-Blandine Martin,¹ Pierre Seneor,¹ Vincent Cros,^{1, b)} Julie Grollier,^{1, c)} and Nicolas Reyren^{1, d)}
Unité Mixte de Physique CNRS, Thales, Univ. Paris-Saclay, 1 Avenue Augustin Fresnel, 91767 Palaiseau, France

Integrating magnetic skyrmion properties into neuromorphic computing promises advancements in hardware efficiency and computational power. However, a scalable implementation of the weighted sum of neuron signals, a core operation in neural networks, has yet to be demonstrated. In this study, we exploit the non-volatile and particle-like characteristics of magnetic skyrmions, akin to synaptic vesicles and neurotransmitters, to perform this weighted sum operation in a compact, biologically-inspired manner. To this aim, skyrmions are electrically generated in numbers proportional to the input with an efficiency given by a non-volatile weight. These chiral particles are then directed using localized current injections to a location where their presence is quantified through non-perturbative electrical measurements. Our experimental demonstration, currently with two inputs, can be scaled to accommodate multiple inputs and outputs using a crossbar array design, potentially nearing the energy efficiency observed in biological systems.

Magnetic skyrmions are topological magnetic solitons behaving like particles. They are stabilized at room temperature in magnetic thin films or heterostructures with optimized magnetic anisotropy and Dzyaloshinskii-Moriya interaction (DMI)¹⁻⁵. Recent experimental studies have shown that magnetic skyrmions can be nucleated^{2,4,6-10}, moved^{2,4,6,7}, annihilated⁹ and electrically detected using the anomalous Hall effect (AHE)¹¹⁻¹³ or tunneling magnetoresistance¹⁴⁻¹⁶. Magnetic skyrmions have a wide span of appealing features that make them prime candidates for energy-efficient computing operations¹⁷⁻¹⁹, such as stability at room temperature, deep sub-micron dimensions, non-volatility, particle-like behavior and motion at low power.

These characteristics align closely with the needs of neuromorphic computing, a discipline aiming to emulate neural network behaviors using in-memory computing to create energy-efficient, artificial intelligence (AI)-specialized hardware²⁰. Recent reports have shown that skyrmions can serve various roles in neuromorphic circuits, from acting as artificial synapses^{19,21} and neurons^{20,22,23} to functioning as stochastic reshufflers^{24,25}. They can even facilitate reservoir computing for data classification based on particle dynamics^{18,26-29}. However, a fundamental neural network operation — the weighted sum of input neuron signals — is still missing in the context of skyrmions²⁰.

As depicted in Fig. 1a, this fundamental operation entails multiplying each input, X_i (where i relates to the index), by a tunable factor known as the synaptic weight, w_i . The subsequent results, Y_i , are then summed to produce the final outcome $Y_{\text{tot}} = \sum_{i=1}^M Y_i = \sum_{i=1}^M w_i X_i$, where M is the number of inputs. Complementary Metal Oxide Semiconductor (CMOS) neuromorphic circuits achieve weighted sums through the combined use of transistors and Static Random Access Memories that have a large silicon footprint (several micrometers

squared per synapse), volatile weights, and consume tens of picoJoules per synaptic operation³⁰. As illustrated in Fig. 1b, biological systems achieve the weighted sum through the nucleation and release of vesicles (black circles) under electrical stimulation, followed by the accumulation and detection of the neurotransmitters that they contain (violet points) to produce the output spikes. They are extremely efficient with non-volatile synapses of sub-micron dimensions, and an energy cost of approximately 25 fJ per synaptic event corresponding to a vesicle release^{31,32}.

In this study, we draw upon biology to design a neuromorphic weighted sum with magnetic skyrmions. The concept is schematized in Fig. 1c. Magnetic skyrmions appear as black dots in the green region that represents the magnetic material where they reside. This material is segmented into distinct tracks, each equipped with a nucleation zone (violet area). When an electrical current pulse is injected along a track with index i , a corresponding number of skyrmions, $N_{\text{Sk}, i}$, is produced in the nucleation zone. The intention is for this number to be proportional to the input values — signified by the current pulse in each track J_i^{In} — multiply by a factor w_i , which represents the weights of the weighted sum: $N_{\text{Sk}, i} = w_i J_i^{\text{In}}$. These skyrmions, once generated, can be displaced under the action of electrical pulses of smaller amplitude through the action of spin-orbit torques (SOT) to accumulate in a specific region (red columns in Fig. 1c), enabling a spatial summation expressed as $N_{\text{Sk}, \text{tot}} = \sum_i N_{\text{Sk}, i}$. The total number of skyrmions in the red region, that can be detected using magneto-resistive means^{11-13,16}, therefore implements the weighted sum of inputs:

$$N_{\text{Sk}, \text{tot}} = \sum_i w_i J_i^{\text{In}} \quad . \quad (1)$$

This approach allows for an electrical readout of the total sum and the eventual application of a subsequent non-linear activation mechanism. In this proposal, the skyrmions take the role of vesicles and neurotransmitters from a biological perspective: they are nucleated and moved in a manner reminiscent of vesicles, but detected and accumulated within neurons in a way analogous to neurotransmitters (see inset of Fig. 1c).

We implement this concept in hardware by using the building block shown in the Kerr microscopy image of Fig. 1d.

^{a)}Present address: Institute of Condensed Matter and Nanosciences, Université catholique de Louvain, Place Croix du Sud 1, 1348 Louvain-la-Neuve, Belgium; tristan.dacamara@uclouvain.be

^{b)}Electronic mail: vincent.cros@cnrs-thales.fr

^{c)}Electronic mail: julie.grollier@cnrs-thales.fr

^{d)}Electronic mail: nicolas.reyren@cnrs-thales.fr

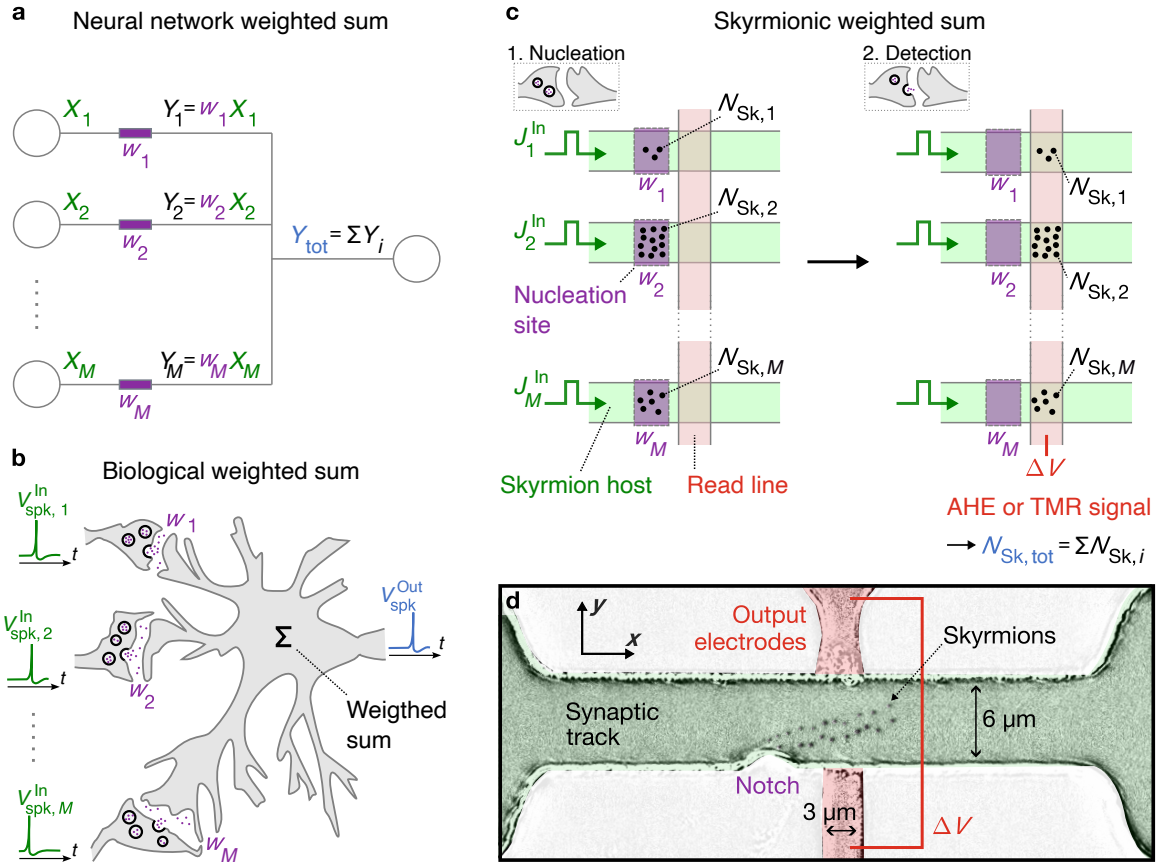


Fig. 1. Skymionic weighted sum: principle and building blocks. **a**, Functioning of a neural network weighted sum that emulates the functionality of the biological one. The input values X_i are multiplied by their respective synaptic weights w_i to generate Y_i values that can be summed to produce an output $Y_{\text{tot}} = \sum_i Y_i$. **b**, Illustration of a biological weighted summation operation within a neuron. The neuron receives spike voltage signals $V_{\text{spk},i}^{\text{In}}$ at various times through synapses, each with its associated synaptic weight w_i . This induces the nucleation and motion of vesicles (black circles) containing neurotransmitters (violet dots). These neurotransmitters accumulate at the neuron receptors, resulting in the weighted summation operation $\sum_i w_i V_{\text{spk},i}^{\text{In}}$. The neuron generates an output spike $V_{\text{spk}}^{\text{Out}}$ when this summation reaches a threshold value, thereby implementing the non-linear activation function. **c**, Illustration depicting the proposed implementation of a skymionic weighted sum, which performs the necessary operation for a neural network weighted sum. Electrical inputs J_i^{In} are applied to skymion host tracks (in green) to nucleate controlled number of magnetic skyrmions $N_{\text{Sk},i}$ at nucleation sites, each with an assigned synaptic weight w_i so that $N_{\text{Sk},i} = w_i J_i^{\text{In}}$. These skyrmions are moved into a transverse electrical detection zone, established by the intersection of the track and the read line for the electrical output (in red), where the cumulative number of skyrmions $N_{\text{Sk,tot}} = \sum_i N_{\text{Sk},i}$ can be electrically detected through an output voltage ΔV arising from the anomalous Hall effect (AHE) or the tunnel magnetoresistance (TMR). The insets highlight the parallel between the biological weighted sum involving the nucleation and motion of vesicles and the accumulation of neurotransmitters. **d**, Kerr microscopy difference image of the device with magnetic skyrmions (dark spots), which were nucleated from a notch in a 6- μm wide synaptic track made of Ta(5 nm)/Pt(8 nm)/[Co(1.2 nm)/Al(3 nm)/Pt(3 nm)]₁₀ multilayer. Skyrmions moved between the detection electrodes made of 3- μm wide and 10-nm thick Ta electrodes connected only at the edges of the track.

The tracks for the skyrmions, colored green in Fig. 1d, contain a skyrmion nucleation site, implemented by a triangular-shape notch. In this system, the skyrmions are detected electrically using AHE and concomitantly counted through Kerr microscopy for validation.

We demonstrate that electrical pulses can nucleate a controllable number of skyrmions from the notch in the host material at room temperature. The number of generated skyrmions directly correlates with the count of applied pulses, allowing efficient input encoding (Eq. 1). The weight factor, influenced by the notch's geometry in the present case, can be adjusted by changing the magnetic field applied on the struc-

ture (but more practical non-volatile solutions exist). We then non-perturbatively detect the nucleated skyrmions using the AHE. Finally, we showcase an experimental demonstration of the weighted sum with a two-input to one-output configuration.

The skymionic weighted sum concept presented in this study offers non-volatile weights and compactness due to fully-electrical, local operations at a submicron scale. We show that the concept is scalable to multiple inputs and outputs by using a crossbar array-like geometry, with the potential of reaching the energy efficiency found in biological systems. We discuss the trade-off between operation precision

and energy expenditure and show that skyrmionic weighted sums with optimized nucleation processes are a promising path to approach the energy efficiency of biological systems.

RESULTS

Electric pulse controlled nucleation and motion of skyrmions

The first experimental challenge to realize the weighted sum is to achieve a precise control of skyrmions nucleation: the quantity of nucleated skyrmions should be directly proportional to the input. This necessitates the development of a reliable method to encode this input within the current pulses that drive the nucleation. Furthermore, the proportionality factor, representing the weight, should be adjustable by modifying properties of the nucleation site to enable learning. The second challenge involves ensuring that all nucleated skyrmions are reliably transported from their nucleation site to the designated accumulation and detection region without loss or gain of skyrmions. The incorporation of detection circuits, as depicted by the red area in Figs. 1c-d, can lead to localized alterations in current density, which can impact the motion of skyrmions. Notably, the Hall cross geometry, which is frequently employed for skyrmion detection, can hinder the movement of some or all skyrmions due to reduced current density at its center.

In our building block shown in Fig. 1d, the tracks for the skyrmions, in green, are 6- μm wide and consist of a magnetic multilayered stack: Ta(5 nm)/Pt(8 nm)/[Co(1.2 nm)/Al(3 nm)/Pt(3 nm)]₁₀ (see Methods for fabrication details). This multilayer stack leverages both interfacial DMI and perpendicular magnetic anisotropy (PMA) allowing to stabilize skyrmions of approximately 200-nm in diameter at room temperature. Furthermore, its composition is tuned to optimize spin-orbit torques, facilitating efficient current-driven skyrmion motion³³. The skyrmion nucleation site, implemented by a rounded triangular notch, accounting for roughly 17% of the track's width. This design enables a local increase in current density, surpassing the threshold for skyrmion nucleation, while ensuring the rest of the track remains below this threshold⁶ (see Supplementary Information S1 for details).

Skyrmion detection is performed through AHE using a specially crafted Hall cross geometry. We design highly-resistive 10-nm thick tantalum (Ta)-based Hall electrodes (measuring 3 μm in width and colored red in Fig. 1d), which are connected solely to its edge (more details in Supplementary Information S1). This minimizes spatial variations of the current density and eliminates potential current leaks that might disrupt skyrmion movement.

The controlled generation of skyrmions by current injection in our building block device is demonstrated in Fig. 2. The track, shown in green in the Kerr microscopy images of Figs. 2a-d, spans 6 μm in width and 40 μm in length, bearing an impedance of 98 Ω including the contacts. It incorporates a nucleation notch as well as a Hall cross. As a preparatory step, we orient the magnetization vertically (along the

+z direction) by applying an out-of-plane (OOP) magnetic field of 200 mT, ensuring complete saturation of magnetization. Subsequently, by injecting current pulses (current density $J = 160 \text{ GA/m}^2$ and pulse duration $t = 50 \text{ ns}$) under an OOP magnetic field ($\mu_0 H_z = 24 \text{ mT}$), we selectively nucleate magnetic skyrmions at the notch. Following their formation, these skyrmions are transported, driven by the spin-orbit torque (SOT) mechanism^{2,4,6}, to the designated detection region (roughly a 6- μm wide square centered between the Ta electrodes in Figs. 2a-d).

The skyrmion count within the track increases linearly with the number of applied current pulses, as demonstrated in Figs. 2a-d. Notably, the skyrmions, being nucleated sequentially, arrange themselves in a linear formation, following an oblique trajectory. This characteristic trajectory can be attributed to the inherent topological properties of skyrmions, specifically the skyrmion Hall effect³⁴. The skyrmion Hall angle, which quantifies the deviation between the current's direction (along x) and the skyrmion's propagation path, is approximately 15°. This value concurs with the anticipated angle for this specific material system at the experimental current density^{6,7}.

To mitigate any potential adverse effects from such transversal motion, the Hall electrodes are positioned close to the notch. This ensures that skyrmions are detected prior to approaching the track's opposite edge, as visualized in Figs. 2a-d. As expected from the skyrmion Hall angle, we determine that skyrmions typically cover a distance of $\sim 15 \mu\text{m}$ longitudinally (in the x direction) before nearing the opposing boundary of the track. By analyzing the skyrmion velocity as a function of the position in the track, we observe that the train of skyrmions can completely cross the area of the Ta-based electrodes without any detectable reduction of their velocity and perturbation of their trajectory. This is due to the much larger sheet resistance of the Ta layer compared to the magnetic multilayer (see Supplementary Information S1 and S2 for more details). In the present device, we find a skyrmion velocity ranging from few m/s to few tens of m/s for current density ranging from 150 to 200 GA/m^2 . The relation between the number of nucleated skyrmions per pulse and the current density displays a quadratic behaviour, which is a signature of a thermally-driven skyrmion nucleation process (see Supplementary Information S3 for details).

Transforming the electrical pulse input into skyrmion number

We demonstrate that our device design allows for the controlled generation of skyrmions and in particular, a linear evolution of their number with the input required to implement the weighted sum operation (Eq. 1). In Figures 2e-f, we display the evolution of the number of nucleated skyrmions N_{SK} in the track observed by Kerr microscopy as a function of the number of current pulses injected in the track N_{Pulses} , under an OOP external magnetic field $\mu_0 H_z = 24 \text{ mT}$.

Our results, presented for varying current pulse densities J in Fig. 2e and different pulse durations t in Fig. 2f, consistently show a direct proportionality between the skyrmion

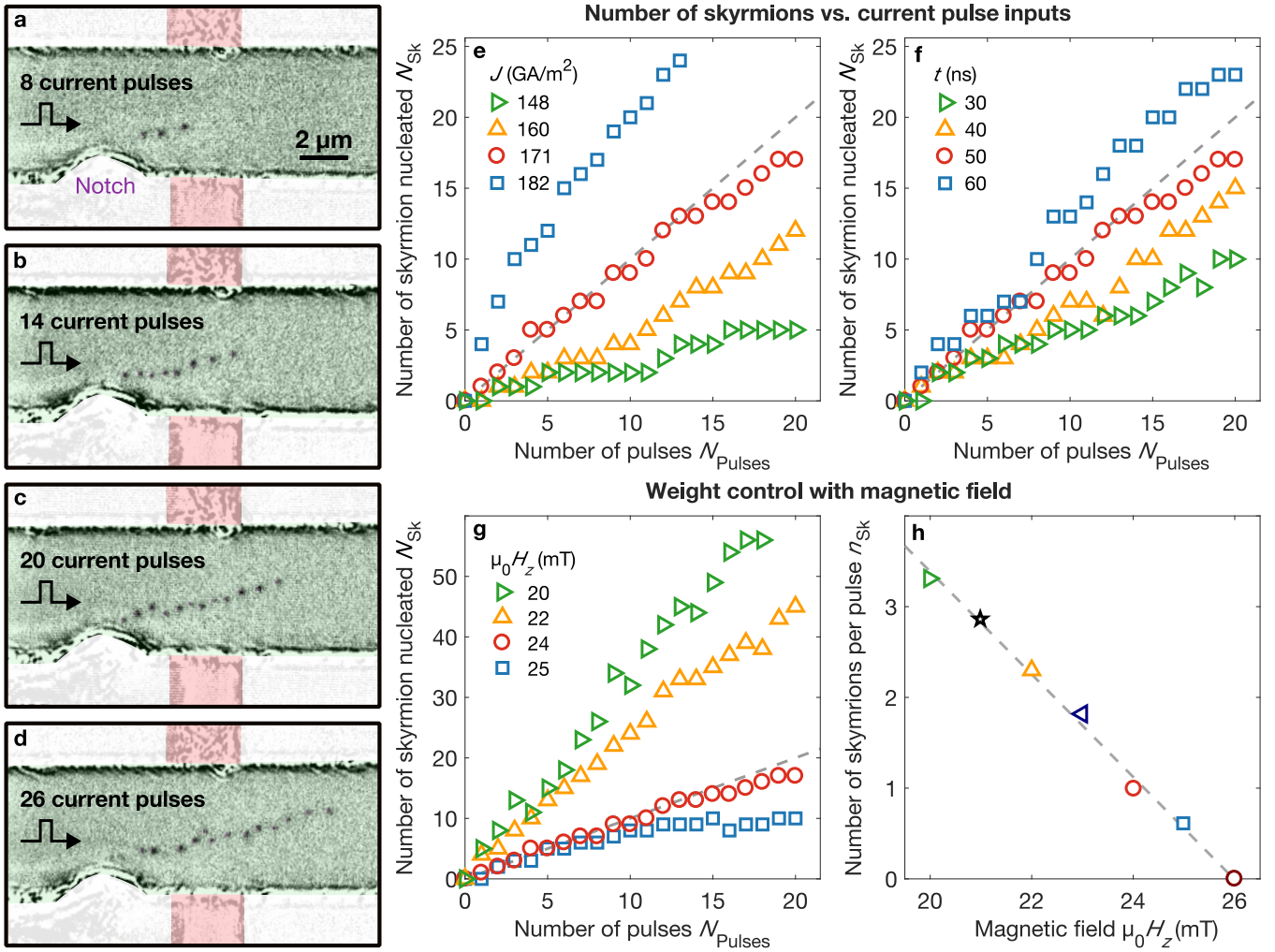


Fig. 2. Controlled nucleation of magnetic skyrmions at a notch using current pulses as inputs and weight fine-tuning. **a-d**, Kerr microscopy images of the device described in Fig. 1d, after the application of 8 **(a)**, 14 **(b)**, 20 **(c)** and 26 **(d)** current pulses with $J = 160 \text{ GA/m}^2$, $t = 50 \text{ ns}$, and under an out-of-plane external magnetic field $\mu_0 H_z = 24 \text{ mT}$. **e-f**, Number of skyrmions nucleated in the track N_{Sk} with the number of pulses applied N_{Pulses} (fixed $\mu_0 H_z = 24 \text{ mT}$) for several current densities J with fixed $t = 50 \text{ ns}$ and **(f)** for several pulse duration t with fixed $J = 171 \text{ GA/m}^2$. **g-h**, Control of the weight using the out-of-plane external magnetic fields H_z . **g**, Number of skyrmions nucleated with the number of pulses N_{Pulses} for several out-of-plane external magnetic fields H_z with fixed $J = 171 \text{ GA/m}^2$ and $t = 50 \text{ ns}$. **h**, Linear control of the number of skyrmions nucleated per pulse (slopes in graphs **e-g**), n_{Sk} , with the magnetic field H_z . The grey dashed lines in **e-g** correspond to 1 nucleated skyrmion per pulse, in **h**, it is a linear fit with a slope of -0.57 skyrmion per pulse and per mT.

count and the number of applied pulses. This underscores our capability to change the number of skyrmions in the track linearly by adjusting the number of input pulses. The nucleation rate of skyrmions per pulse also displays a linear relationship with pulse duration (as described in Supplementary Information S3, Fig. S4), offering an alternative to the number of current pulses to encoded the input.

For specific parameter sets, e.g. $J = 171 \text{ GA/m}^2$ and $t = 50 \text{ ns}$, we observe a one-to-one ratio of skyrmion to pulse (highlighted by the grey dashed lines in Figs. 2e-f). By modulating these parameters, we can control nucleation probabilities, thus achieving a desired skyrmion number in the track. This flexibility allows for either a small number of skyrmions, facilitating optical detection, or a higher number of skyrmions, suitable for more complex operations. The lat-

ter is particularly valuable for addressing device sensitivity issues that may arise from small variations in skyrmion numbers or to reduce potential computation errors caused by unintended skyrmion nucleation or annihilation. Furthermore, a high skyrmion count also improves the electrical signal, making easier the electrical detection.

Magnetic field control of the synaptic weight

In Fig. 2g, we show that the proportionality factor between the number of nucleated skyrmions N_{Sk} and the number of current pulses injected N_{Pulses} , which in our concept defines the synaptic weight, depends on the amplitude of the external perpendicular magnetic field H_z . These results demonstrate

that the synaptic weight can be tuned by an external OOP magnetic field. The smaller the value of the external magnetic field H_z , the larger is the number of nucleated skyrmions for a given current pulse. Notably, more than 50 skyrmions can be nucleated in the 6- μm wide track in 20 current pulses ($J = 171 \text{ GA/m}^2$ and $t = 50 \text{ ns}$) by decreasing the magnetic field to 20 mT. Depending on the application, the number of states could be adjusted by the skyrmion diameter relative to the track width.

In Fig. 2h, we present the number of skyrmions nucleated per current pulse, or nucleation probability $n_{\text{Sk}} = dN_{\text{Sk}}/dN_{\text{Pulses}}$ extracted from linear fits in Fig. 2g as a function of H_z . This nucleation probability is found to decrease linearly with H_z . A variation of about -0.57 skyrmions per pulse and per mT is found up to a maximum field $\mu_0 H_{z,\text{max}} = 26 \text{ mT}$, where no more skyrmion is nucleated (for fixed $J = 171 \text{ GA/m}^2$ and $t = 50 \text{ ns}$). On the contrary, if the field is further reduced below 20 mT, elongated domains are found to be nucleated in the track, thus setting a minimal field for device operation.

Our findings indicate that adjusting the magnetic properties at the nucleation site can effectively modulate the synaptic weight. In prospective devices, achieving such modifications could be realized in a non-volatile and local way, possibly leveraging magneto-ionic effects, as elaborated upon in the discussion section.

Neuronal detection and output: non-perturbative electrical detection of the skyrmion number

As described before, the final summation in our device corresponds in practice to the measurement of the anomalous Hall voltage across the detection area in which skyrmions have been accumulated. For this purpose, a small dc current of $100 \mu\text{A}$ ($J = 0.21 \text{ GA/m}^2 \ll J_{\text{nucleation}}$) is applied along the track, and the transverse voltage, directly proportional to the mean magnetisation along the z direction, is measured (see Supplementary Information S2, Figs. S3a-b for the Hall voltage hysteresis loops).

The variation in Hall voltage is shown in Fig. 3, denoted as ΔV , as skyrmions are introduced into the detection zone (highlighted by the blue dotted square in Fig. 3). This variation is displayed under three distinct combinations of magnetic fields and currents. The x-axis, titled ‘‘measurement iteration’’, represents consecutive measurement sequences. Initially, 10 voltage measurements are taken without any skyrmion injections to determine the saturated voltage value, meaning when no skyrmions are present. In the depicted graph, these initial 10 data points exhibit a consistent Hall voltage, with $\Delta V \approx 0$. Following this, 20 current pulses are used to nucleate skyrmions, which is represented by the green area in Fig. 3. After each pulse, both the Hall voltage and a Kerr image are recorded. As visible in Fig. 3, for each set of conditions, ΔV rises due to the accumulated skyrmions in the detection zone. To conclude the measurement sequence, a strong saturating field of 200 mT is applied to reset the system (eliminates all the skyrmions). The final 10 voltage measurements, corre-

sponding to the concluding data points on the graph, revert to $\Delta V \approx 0$. Reversing the current pulse direction is another way to erase skyrmions one by one: the skyrmions move back along the same trajectory and get annihilated at the notch.

In Fig. 3, each skyrmion represents a consistent opposite z magnetisation contribution compared to the saturated state¹¹. This means the Hall voltage variation, ΔV , can be directly associated with the number of skyrmions present in the detection zone, denoted as $N_{\text{Sk, detec}}$. Alongside the Hall measurements in Fig. 3, we also plot the number of skyrmions identified in the detection zone via Kerr imaging (illustrated in the insets). We base our analysis on the assumption that the AHE is proportional to the z -component of the magnetisation distribution within a 6- μm^2 square centered on the Hall bar, as marked by the dashed blue outlines in the insets. Skyrmions further away from this center are excluded from consideration. This methodological choice is supported by experimental data showing a proportional relationship between ΔV values and the count of skyrmions derived from the magneto-optic Kerr images. Notably, the ratio of the scales on the y-axes of Figs. 3a-c are constant across all plots. This showcases the concomitant increase in both skyrmion counts and ΔV values with either increasing pulse current density (as seen in Figs. 3a-b) or decreasing OOP external magnetic field intensity H_z (as seen in Figs. 3b-c). Given the limited size of the detection zone, both the skyrmion count and the resultant Hall voltage eventually plateau as the detection area becomes saturated or skyrmions begin to move beyond its boundaries.

From our measurements, we deduce a contribution of approximately 22 nV to the Hall voltage variation for each skyrmion (using a dc current of $100 \mu\text{A}$) with a standard deviation of 7 nV (see Supplementary Information S4). This finding is in line with data presented by Maccariello et al. in Ref. 11. Additionally, by analyzing the Hall voltage shift when the magnetization of the detection zone undergoes a full reversal (see Supplementary Information S2, Fig. S3b) and assuming that skyrmions can be represented as circular domains with a uniform, opposite ‘‘down’’ magnetization, we estimate the skyrmion diameter to be approximately $222 \pm 33 \text{ nm}$. This estimation agrees well with observations made using magnetic force microscopy (MFM) on similar tracks (not shown). Collectively, these results demonstrate the capability of electrically counting skyrmions with high precision using AHE, a crucial aspect for executing the neuromorphic weighted sum operation.

Demonstration of the weighted sum operation

In this section, we present the weighted sum operation using a configuration with two inputs and one output. The device, shown in Fig. 4a, consists of two parallel magnetic multilayered tracks, each 6- μm wide and equipped with a nucleation notch. These tracks are intersected by a 6- μm wide Ta Hall electrode. The details of the measurement circuit for AHE detection in this configuration are given in Methods.

A current pulse generator is connected to the track 1, then to the track 2, to successively inject skyrmions in both tracks

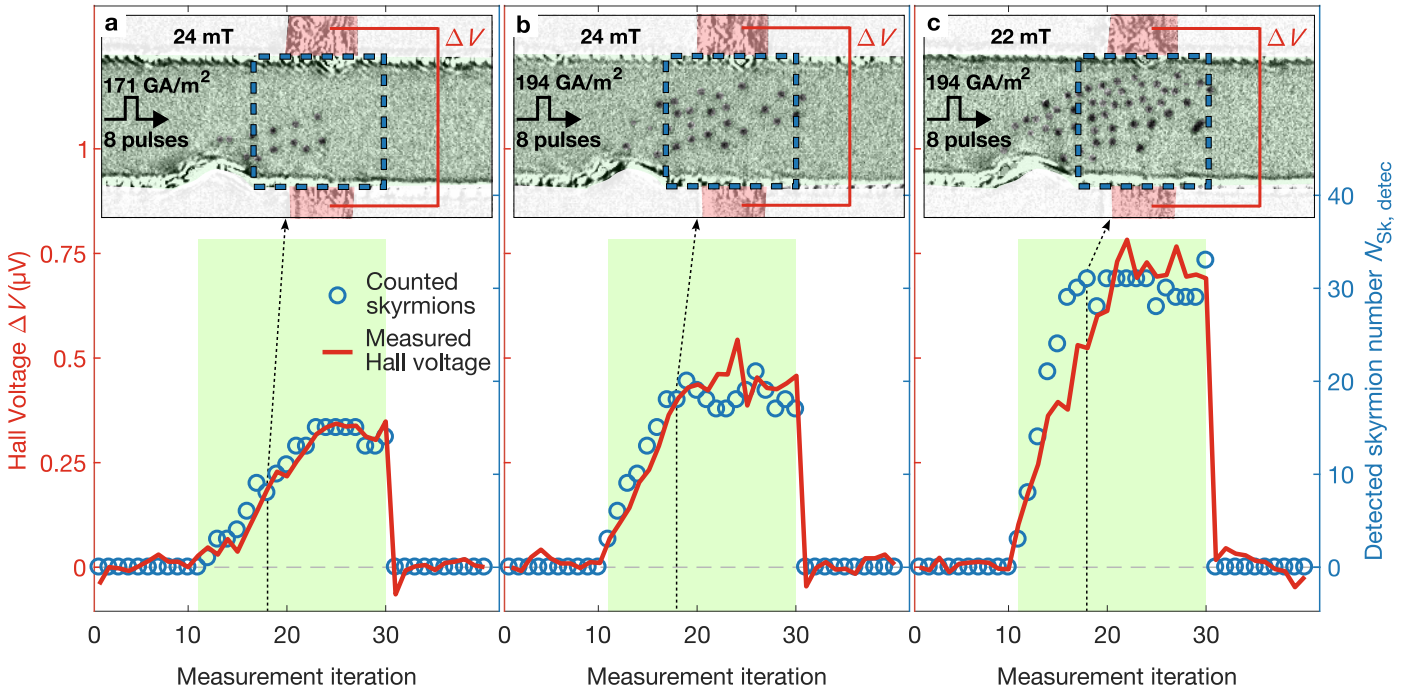


Fig. 3. Non-perturbative electrical detection of the number of skyrmions using thin Ta electrodes. a-c, Evolution of the Hall voltage $\Delta V = V - V_{\text{sat}}$ and the number of detected skyrmions $N_{\text{Sk, detec}}$ as a function of measurement index (1 pulse applied before each measurements with indices 11 to 30) for pulses with $J = 171 \text{ GA/m}^2$ (a), 194 GA/m^2 (b-c) (fixed $t = 50 \text{ ns}$) and $\mu_0 H_z = 24 \text{ mT}$ (a-b) and 22 mT (c). Ten measurements of the voltage are performed before the application of the pulses and after magnetically erasing the skyrmions, defining V_{sat} . The green areas indicate the application of the current pulses. Insets in a-c: corresponding Kerr microscopy images of the nucleated skyrmions after 8 current pulses applied in the different conditions. The blue dashed boxes indicate the detection zone estimated as a $6\text{-}\mu\text{m}$ wide square.

(Figs. 4b and c), before reset, i.e., erasing the skyrmions by applying an external magnetic field $\mu_0 H_z = 200 \text{ mT}$ (Fig. 4d). The corresponding Hall voltage variation ΔV for current pulses of about 116 GA/m^2 and 50 ns with $\mu_0 H_z = 20 \text{ mT}$ is shown in Fig. 4e. The measurement sequence is the same as for the individual track i.e. 20 measurements of the Hall voltage are taken after fully saturating the tracks' magnetisation and a Kerr image is taken as reference. Then, 20 pulses are applied to track 1, each pulse being followed by a voltage measurement, while Kerr images are taken after every 5 pulses. This results in the concomitant increase of the skyrmions number detected in track 1 (blue dots in the green area of Fig. 4e) with the Hall voltage (red line). 20 more voltage measurements are carried out to check the voltage stability. The same process is then repeated for track 2, which leads to a further increase of both the total detected skyrmion number and the Hall voltage. The Hall voltage variation measured for each successive skyrmion injection corresponds well to the value expected from individual measurements of the two Hall crosses (see Supplementary Information S5, Figs. S6c-j). This result demonstrates that the measured Hall voltage ΔV is, as desired for the final sum operation of our device, directly proportional to the sum of the skyrmion numbers in the two tracks.

This device produces the same weight for each track as the notches are nominally identical, and the external OOP magnetic field is the same over the entire structure. To study the

evolution of the AHE voltage for different weights in each track, we can however modulate the weight - i.e. the number of skyrmions generated by each pulse - by changing the duration of the pulse (Supplementary Information S5: the linear evolution of the number of skyrmions and the related Hall voltage with pulse duration is shown in Figs. S6c-j). In Figs. 4f-g, we illustrate this control. In each case, we keep constant the number of current pulses (30), the current density $J = 116 \text{ GA/m}^2$, and the external field $\mu_0 H_z = 20 \text{ mT}$, but the pulse duration is varied. In Fig. 4f, the same pulse duration $t = 50 \text{ ns}$ is used in the two tracks, corresponding to identical weights. Once again, this results in two consecutive and identical increases in the Hall voltage, with the mean Hall voltage measuring $105 \pm 15 \text{ nV}$ and $211 \pm 16 \text{ nV}$ following nucleation in track 1 and track 2, respectively. In Fig. 4g, the pulse duration is reduced to $t = 30 \text{ ns}$ for injecting skyrmions in the track 2, corresponding to reducing the weight close to zero in this track (Supplementary Information S5, Figs. S6h and j). As expected, the resulting average Hall voltage after the injection in track 2 ($147 \pm 29 \text{ nV}$) is almost unchanged compared to the value obtained after the nucleation in track 1 ($121 \pm 27 \text{ nV}$). This is indeed equivalent to a suppression of the second term related to track 2 by setting $w_2 \approx 0$, while keeping w_1 unchanged, in the total output signal $\Delta V = w_1 N_{\text{Pulse},1} + w_2 N_{\text{Pulse},2}$. The Kerr image reproduced in Fig. 4h explains that in the latter case the detected skyrmion number is close to zero in Track 2 (only side effects).

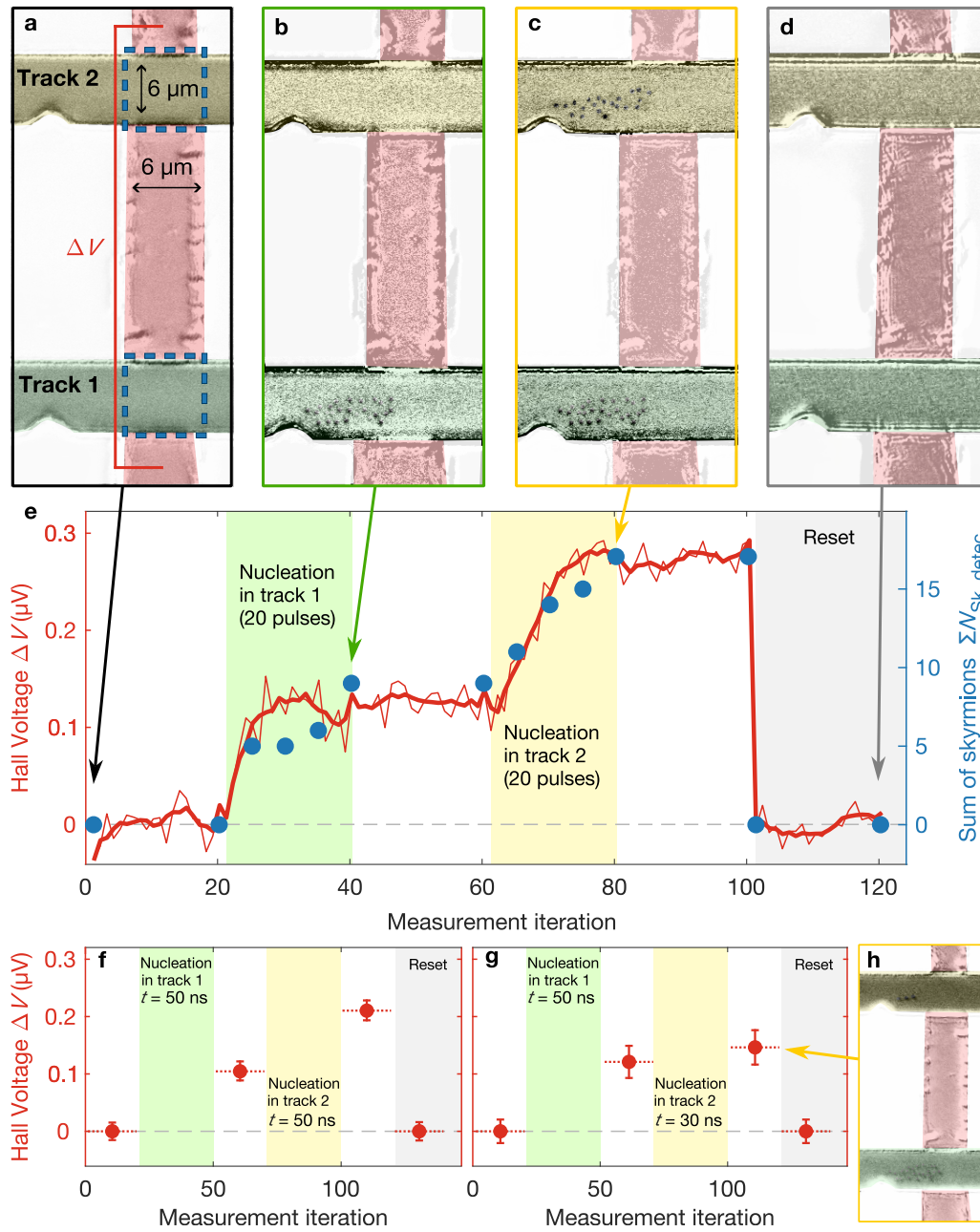


Fig. 4. Weighted sum in a device composed of two parallel multilayer tracks. **a-d**, Kerr microscopy images of the device composed of two 6- μm wide parallel magnetic multilayer tracks connected by a transverse 6- μm wide Ta Hall electrode. After the saturation of the track using $\mu_0 H_z = 200$ mT (**a**), skyrmions can be selectively nucleated in track 1 (**b**) and track 2 (**c**), before being erased by another $\mu_0 H_z = 200$ mT (**d**). **e**, Hall voltage ΔV (in red) and the corresponding sum of the skyrmion number detected in both tracks $\sum N_{\text{Sk, detec}}$ (in blue) for successive injection of skyrmion in the tracks. 20 nucleation pulses are successively applied to each track (indicated by the green and yellow areas for track 1 and 2 respectively) using current pulse of about 116 GA/m^2 and 50 ns, at $\mu_0 H_z = 20$ mT. The thin red curve represents the raw electrical measurements after correction of the drift, while the thick one is the same after smoothing. **f-g**, Mean value of the Hall voltage ΔV after 30 nucleation pulses successively applied to each track, where the pulse duration applied to track 2 is reduced from 50 ns (**f**) to 30 ns (**g**). **h**, Kerr microscopy images corresponding to the measurement (**g**).

DISCUSSION

Scaling

The neuromorphic weighted sum device can be scaled to accommodate more inputs and outputs using a crossbar ar-

ray geometry, as illustrated in Fig. 5a. By adding more input tracks to a device like the one shown in Fig. 4, the system can linearly scale: for instance, M parallel tracks can support a weighted sum of M inputs. To increase the number of outputs to L , additional notches and Hall bars along the track can

be introduced. Utilizing high-resistivity electrodes for AHE measurements, such as the Ta used in our study, can mitigate issues like current leaks and sneak paths that are common in traditional crossbar arrays with oxide materials and conductive electrodes. The non-linear activation function can be applied to the resulting AHE voltage ΔV by leveraging CMOS technology, which is compatible with our device.

As an alternative to Hall bars, magnetic tunnel junctions (MTJ) could be employed for electrical skyrmion detection through their tunnel magnetoresistance (TMR) ratio instead of relying on Hall voltages. The device concept is schematically illustrated in Fig. 5a. A large TMR ratio, akin to those in MRAM MTJ bits, could provide a more robust output signal, simplifying on-chip detection circuits. Notably, the TMR signal is expected to monotonically increase with the cumulative number of skyrmions beneath the MTJ, and to introduce the necessary non-linearity, especially for largest TMR. Consequently, using MTJs as skyrmion detectors can intrinsically apply the non-linear activation function of the neurons directly at the crossbar outputs. This approach has the potential to execute all essential neuromorphic computing operations within a single device, eliminating the need for external electrical interconnections between the individual components of the neural layer.

In our demonstration, the input is coded by the number of current pulses directed to a track, and the Hall voltage serves as the output signal. For future integration of multiple crossbar arrays, it would be beneficial to use consistent types of inputs and outputs. One promising direction is the use of new spin or orbital torques for skyrmion nucleation³⁵, rather than the thermal effects utilized in our present approach. These torques should also result in a linear correlation between the current density and the number of skyrmions. In such a scenario, the amplitude of the current pulses could act as an input parameter. Conveniently, conversions between such inputs and outputs could be efficiently executed in CMOS using straightforward amplification using transistors. Another promising approach involves utilizing voltage-controlled magnetic anisotropy (VCMA) to induce skyrmion nucleation by applying gate voltage within the nucleation sites^{16,36}. In this scenario, the inputs are directly encoded in voltage amplitudes, ensuring direct consistency with the output voltages.

Tunable weights

Our experimental proof of concept device features fixed weights, but we have shown that these weights can be tuned by modifying local magnetic properties at the nucleation sites. A viable approach for developing miniature trainable devices involves leveraging magneto-ionic effects. By applying electric field gating, these effects can induce local, non-volatile, and reversible alterations to the magnetic anisotropy and Dzyaloshinskii-Moriya interaction within the magnetic multilayer stack³⁷⁻⁴². Such modifications enable tuning of skyrmion nucleation³⁶ and dynamics^{43,44}, effectively adjusting the synaptic weights. The observed linear correlation

between the number of nucleated skyrmions and the OOP external magnetic field, as seen in Fig. 2h, implies a potential linear relationship between the number of nucleated skyrmions and the sample's anisotropy field. This suggests a straightforward calibration of the synaptic weights. It is worth noting that the gate employed for the magneto-ionic modification of magnetic properties can also serve for VCMA-induced skyrmion nucleation with significantly reduced energy requirements^{16,36}. This could be achieved by leveraging different timescales for VCMA nucleation of skyrmions and the voltage gate-induced ionic motion used for weight modification. Figure 5a also provides a schematic representation of the nucleation site design for VCMA-based nucleation and weight control.

Energy of synaptic operation

The energy for our proposed skyrmionic weighted sum is determined by the nucleation energy of a skyrmion. We experimentally demonstrate this sum operation using a thermal nucleation scheme⁶, related to a temperature increase by about $\Delta T \approx 100$ K. $E_{th} = C\mathcal{V}\Delta T \approx 10$ pJ/skyrmion, where C is the volumetric specific heat and \mathcal{V} is the smallest volume heated to nucleate one skyrmion. Reducing the metallic volume to be heated can further decrease E_{th} to the pJ/skyrmion range. In our experimental device, the heat energy is provided by a current pulse and has been estimated to be approximately 20 pJ/skyrmion (see Supplementary Information Section S6). This value corresponds well to the expected thermal energy required for the nucleation of a skyrmion.

Efficient nucleation techniques, such as VCMA, can potentially lower nucleation energy to just under 100-fJ, based on recent MTJ experiments¹⁶. VCMA devices, given their input and weight encoding, promise significant energy savings per synaptic event compared to neuromorphic CMOS chips (~ 10 pJ/synaptic event³⁰), with the added benefit of weight retention. Remarkably, this is close to the energy consumption of a biological synaptic event, approximately ~ 25 fJ, associated with vesicle release³¹, underscoring the potential of skyrmions for brain-equivalent efficiency in neuromorphic computing.

Reliability of the sum operation

In this section, we address the question of the reliability of the sum operation. The nucleation of the skyrmion being of thermal origin, the process is stochastic and, if the system is tuned to produce 1 skyrmion per electrical pulse, the outcome can be different than one with a probability $p(\bar{1})$. In our experimental devices, we observe the nucleation of zero, one or two skyrmions when the current pulses are shaped to create a single skyrmion/pulse in average. We have performed numerical simulations for several values of $p(1)$ to determine the relative deviation σ of the number of nucleated skyrmion N_{Sk} for N_{Pulse} electrical pulses (see Supplementary Information Section S7 for details). The results are plotted in Fig. 5b

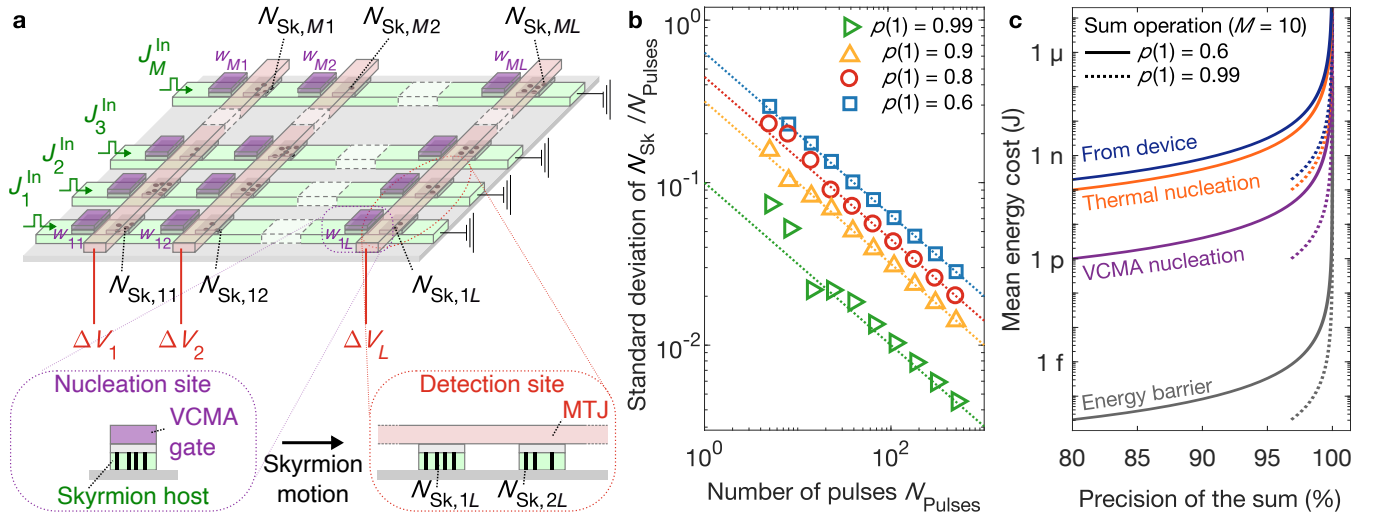


Fig. 5. Schematic and characteristics of an expanded neuromorphic computing device. **a**, Crossbar architecture comprising M parallel tracks (in green) intersected by L Magnetic Tunnel Junctions (MTJ, in red). It enables the introduction of M electrical inputs to inject skyrmions from each nucleation site made of voltage-controlled magnetic anisotropy (VCMA) gate (in purple). The skyrmions are then moved into the detection sites where their number naturally sum, inducing L electrical output voltages. The output voltage produced on column j is given by $\Delta V_j = f[\sum_i N_{Sk,ij}] = f[\sum_i (w_{ij} N_{Pulse\ i})]$, where i is the track index and f reflects the non-linear activation function of the MTJ applied to the sum of the skyrmion number $\sum_i N_{Sk,ij}$. **b**, Evolution of the standard deviation σ of the nucleated number of skyrmion N_{Sk} over the number input pulses N_{Pulse} as a function of N_{Pulse} for a single synapse and for several value of the probability of nucleating one skyrmion $p(1)$. The larger the number of attempted skyrmions or the larger $p(1)$, the smaller the relative error with $\sigma \approx \sqrt{(1-p(1))/N_{Pulse}}$. **c**, Estimated mean energy cost in a device composed of 10 synapses as a function of the desired weighted sum precision considering the energy to nucleate a single skyrmion as ~ 20 pJ (estimate from the device in Fig. 2), 10 pJ (thermally induced nucleation), 100 fJ (VCMA induced nucleation) and $500k_B T \approx 2$ aJ at $T = 300$ K (energy barrier for stable skyrmions).

assuming that $p(0) = p(2) = p(\bar{1})/2$. They show an excellent agreement with the formula $\sigma \approx \sqrt{p(\bar{1})/N_{Pulse}}$. In our experimental device, we estimate $p(1)$ to be approximately 0.6, a number which also accounts for the detection noise (see Supplementary Information Section S7 for all details). This number is comparable to the probability of vesicle release in biology (corresponding to the skyrmion nucleation in our concept) typically between 0.25 to 0.5³².

The precision of the sum operation is set by this nucleation probability. When M independent synapses produce each one $N_{Sk,m}$, the expected standard deviation of the sum, $\sqrt{\sum_{m=1}^M \sigma^2(m)}$, is equal to $\sqrt{M}\sigma$ if all synapses have the same standard deviation. When N_{Pulse} are injected per synapse, the sum is equal to MN_{Pulse} , the precision of the sum is given by $1 - \sigma(N_{Pulse})/\sqrt{M} = 1 - \sqrt{p(\bar{1})}/(MN_{Pulse})$ and the mean energy cost is MN_{Pulse} times the estimated energy needed to nucleate a skyrmion. In Fig. 5c, we depict the relationship between the precision of the sum and the mean energy cost. As seen, achieving higher precision necessitates greater energy consumption. Consequently, an optimal operating point can be identified by balancing energy cost against sum precision requirements akin to a trade-off encountered in biology³². Two alternative paths for device optimization are (1) to encode numbers with larger number of skyrmions, or (2) to improve the deterministic nucleation of skyrmions. Other nucleation schemes, for example inspired by MRAM technologies, might reduce $p(\bar{1})$ by many orders of magnitude.

CONCLUSION

We propose an experimental proof of concept for a large scale, low energy consumption hardware weighted sum based on magnetic skyrmions. We first demonstrate a method for electrically controlling skyrmion nucleation and movement within specially crafted magnetic multilayered tracks. The linear association between the number of generated skyrmions and applied current pulses, under various parameter sets, highlights the precision of the method, and implements the multiplication of the inputs by a synaptic weight. The weight can be finely tuned through minor adjustments to the out-of-plane external magnetic field (close to -0.57 skyrmions per pulse and per mT). Utilizing optimized parameters, we achieve the injection of over 50 skyrmions into a 6- μ m wide track. Our design employs highly resistive Ta transverse electrodes connected to the edge of the track only, enabling the electrical detection of skyrmions via the anomalous Hall effect without adversely affecting their motion or providing sneak paths in crossbar arrays. We validate the weighted sum operation in a device featuring two parallel tracks intersected by a Hall electrode; the resulting Hall voltage corresponds to the combined number of skyrmions in both tracks. This ensures efficient execution of the fundamental weighted sum operation, a cornerstone for neuromorphic computing.

Looking forward, integrating magneto-ionic effects for non-volatile, reversible control over local magnetic properties, along with non-linear electrical detection via magnetic tun-

nel junctions, promises comprehensive functionality for neuromorphic computing. These advancements pave the way for brain-inspired hardware capable of weighted sums at an energy expenditure as minimal as 1-100 aJ per synaptic operation.

METHODS

Device fabrication

The samples Ta(5 nm)/Pt(8 nm)/[Co(1.2 nm)/Al(3 nm)/Pt(3 nm)]₁₀, with the index '10' signifying ten repetitions of the trilayer, are grown by magnetron sputtering at room temperature on Si₃N₄ substrates. The device geometries are defined by a three steps UV lithography process. A first step is used to define the 6- μ m wide track geometry with the notch as well as contacts for the Hall electrodes, which is obtained by Ar⁺ ion etching of the multilayer film. A second step is used to define the crossing Hall bar electrodes, still by UV lithography, while keeping the resist mask used for the first step to ensure that the electrodes are only connected on the edge of the multilayer track. The 10-nm thick Ta electrodes are then deposited by sputtering and lifted-off. Finally, a third lithography step is used to lift-off sputtered Ti (10 nm)/Au (200 nm) electrical contacts for electrical measurements.

Kerr microscopy

Kerr microscopy is used to observe and count the skyrmions in the devices. For each measurement series, a reference image is taken in the saturation state and subtracted to the displayed image. This image difference enhances the magnetic contrast, and reduces the "topographical" features. The light source is a blue light emitting diode (LED) with a peak intensity at 445 nm wavelength. For the maximum resolution, we use a 100x lens in immersion in a high refraction index oil ($n = 1.5$) and large numerical aperture (1.3). Due to thermal drifts, the sample is realigned before each image using a 3D piezoelectric stage. The focus is a key parameter to get the contrast of the sub-wavelength diameter skyrmions. A fine focus series of images is taken varying the focus in order to achieve maximum resolution. The best-focused image is automatically selected, and its optimized focus position is then forwarded for the next image acquisition. Due to this procedure, each acquisition takes typically a few minutes. A final fine correction for the drift in planar directions is made in post-treatment.

The color of the Kerr images presented in this work have been modified to improve the readability of the figures, the Kerr images without color modifications are provided in the Supplementary Information Section S8.

Electrical measurements

Skyrmions are nucleated and moved using pulses generated by an arbitrary waveform generator connected to a 38 dB amplifier, typical voltages are in the volt range. The Hall voltage measurements are performed by using a dc current source and a nanovoltmeter to measure the transverse Hall voltage with 100 μ A. This current corresponds to a current density in the range of 0.1 GA/m², which is about three orders of magnitude below the threshold current for skyrmion nucleation and motion. To improve the electrical measurement precision, each voltage measurement is the average of 50 individual pair of measurements with positive and negative 100 μ A current with duration of 100 ms. AHE loop measurements are obtained by sweeping an OOP external magnetic field and recording the Hall voltage to which an offset is subtracted. The offset corresponds to a small longitudinal voltage component (see Supplementary Information S2, Fig. S3).

For the measurements of a single device composed of parallel multilayer tracks, the tracks are connected in parallel to a dc current source. Track 1 and 2 have respectively a resistance value of 130 Ω and 120 Ω . Each track has 12 k Ω calibrated resistances in series at each end of each track. This ensures identical (within 0.1%) dc current of 100 μ A flowing in each track. Moreover, it guarantees that the voltage measured at the edge of the Hall cross only arises from the device instead of the electrical circuit used for the measurement (see Supplementary Information S5, Fig. S6a for a schematics of the electrical circuit). With this circuit, the Hall voltage measurement is found to be, indeed, the sum of the individual Hall voltage of each individual track (see Supplementary Information S5, Fig. S6b). This indicates that the Hall voltage measured at the edge of the device accounts for the sum of the magnetisation contribution of the two Hall crosses. Bias Tees are used to selectively inject current pulses or dc current within the desired track.

The quoted current densities are the averaged ones estimated by dividing the total current by the width of the track (6 μ m) and the total magnetic multilayer thickness (85 nm).

REFERENCE

- ¹C. Moreau-Luchaire, C. Moutafis, N. Reyren, J. Sampaio, C. A. F. Vaz, N. Van Horne, K. Bouzehouane, K. Garcia, C. Deranlot, P. Warnicke, P. Wohlhüter, J. M. George, M. Weigand, J. Raabe, V. Cros, and A. Fert, "Additive interfacial chiral interaction in multilayers for stabilization of small individual skyrmions at room temperature," *Nature Nanotechnology* **11**, 444–448 (2016).
- ²W. Jiang, P. Upadhyaya, W. Zhang, G. Yu, M. B. Jungfleisch, F. Y. Fradin, J. E. Pearson, Y. Tserkovnyak, K. L. Wang, O. Heinonen, S. G. E. te Velthuis, and A. Hoffmann, "Blowing magnetic skyrmion bubbles," *Science* **349**, 283–286 (2015).
- ³G. Chen, A. Mascaraque, A. T. N'Diaye, and A. K. Schmid, "Room temperature skyrmion ground state stabilized through interlayer exchange coupling," *Applied Physics Letters* **106**, 242404 (2015).
- ⁴S. Woo, K. Litzius, B. Krüger, M.-Y. Im, L. Caretta, K. Richter, M. Mann, A. Krone, R. M. Reeve, M. Weigand, P. Agrawal, I. Lemesch, M.-A. Mawass, P. Fischer, M. Kläui, and G. S. D. Beach, "Observation of room-

- temperature magnetic skyrmions and their current-driven dynamics in ultrathin metallic ferromagnets,” *Nature Materials* **15**, 501–506 (2016).
- ⁵O. Boulle, J. Vogel, H. Yang, S. Pizzini, D. de Souza Chaves, A. Locatelli, T. O. Menteş, A. Sala, L. D. Buda-Prejbeanu, O. Klein, M. Belmeguenai, Y. Roussigné, A. Stashkevich, S. M. Chérif, L. Aballe, M. Foerster, M. Chshiev, S. Auffret, I. M. Miron, and G. Gaudin, “Correction: Corrigendum: Room-temperature chiral magnetic skyrmions in ultrathin magnetic nanostructures,” *Nature Nanotechnology* **12**, 830–830 (2017).
- ⁶W. Legrand, D. Maccariello, N. Reyren, K. Garcia, C. Moutafis, C. Moreau-Lucaire, S. Collin, K. Bouzehouane, V. Cros, and A. Fert, “Room-temperature current-induced generation and motion of sub-100 nm skyrmions,” *Nano Letters* **17**, 2703–2712 (2017).
- ⁷A. Hrabec, J. Sampaio, M. Belmeguenai, I. Gross, R. Weil, S. M. Chérif, A. Stashkevich, V. Jacques, A. Thiaville, and S. Rohart, “Current-induced skyrmion generation and dynamics in symmetric bilayers,” *Nature Communications* **8**, 15765 (2017).
- ⁸F. Büttner, I. Lemesch, M. Schneider, B. Pfau, C. M. Günther, P. Hensing, J. Geilhufe, L. Caretta, D. Engel, B. Krüger, J. Viehhaus, S. Eisebitt, and G. S. D. Beach, “Field-free deterministic ultrafast creation of magnetic skyrmions by spin-orbit torques,” *Nature Nanotechnology* **12**, 1040–1044 (2017).
- ⁹S. Woo, K. M. Song, X. Zhang, M. Ezawa, Y. Zhou, X. Liu, M. Weigand, S. Finizio, J. Raabe, M.-C. Park, K.-Y. Lee, J. W. Choi, B.-C. Min, H. C. Koo, and J. Chang, “Deterministic creation and deletion of a single magnetic skyrmion observed by direct time-resolved x-ray microscopy,” *Nature Electronics* **1**, 288–296 (2018).
- ¹⁰S. Finizio, K. Zeissler, S. Wintz, S. Mayr, T. Weßels, A. J. Huxtable, G. Burnell, C. H. Marrows, and J. Raabe, “Deterministic field-free skyrmion nucleation at a nanoengineered injector device,” *Nano Letters* **19**, 7246–7255 (2019).
- ¹¹D. Maccariello, W. Legrand, N. Reyren, K. Garcia, K. Bouzehouane, S. Collin, V. Cros, and A. Fert, “Electrical detection of single magnetic skyrmions in metallic multilayers at room temperature,” *Nature Nanotechnology* **13**, 233–237 (2018).
- ¹²K. Zeissler, S. Finizio, K. Shahbazi, J. Massey, F. A. Ma’Mari, D. M. Bracher, A. Kleibert, M. C. Rosamond, E. H. Linfield, T. A. Moore, J. Raabe, G. Burnell, and C. H. Marrows, “Discrete hall resistivity contribution from néel skyrmions in multilayer nanodiscs,” *Nature Nanotechnology* **13**, 1161–1166 (2018).
- ¹³S. Wang, J. Tang, W. Wang, L. Kong, M. Tian, and H. Du, “Electrical detection of magnetic skyrmions,” *Journal of Low Temperature Physics* **197**, 321–336 (2019).
- ¹⁴C. Hanneken, F. Otte, A. Kubetzka, B. Dupé, N. Romming, K. von Bergmann, R. Wiesendanger, and S. Heinze, “Electrical detection of magnetic skyrmions by tunnelling non-collinear magnetoresistance,” *Nature Nanotechnology* **10**, 1039–1042 (2015).
- ¹⁵H. Chen, W. Bouckaert, and S. A. Majetich, “Tunnel magnetoresistance detection of skyrmions,” *Journal of Magnetism and Magnetic Materials* **541**, 168552 (2022).
- ¹⁶J. U. Larrañaga, N. Sisodia, V. T. Pham, I. D. Manici, A. Masseboeuf, K. Garello, F. Disdier, B. Fernandez, S. Wintz, M. Weigand, M. Belmeguenai, S. Pizzini, R. Sousa, L. Buda-Prejbeanu, G. Gaudin, and O. Boulle, “Electrical detection and nucleation of a magnetic skyrmion in a magnetic tunnel junction observed via operando magnetic microscopy,” (2023), arXiv:2308.00445 [cond-mat.mtrl-sci].
- ¹⁷A. Fert, N. Reyren, and V. Cros, “Magnetic skyrmions: advances in physics and potential applications,” *Nature Reviews Materials* **2**, 17031 (2017).
- ¹⁸G. Bourianoff, D. Pinna, M. Sitte, and K. Everschor-Sitte, “Potential implementation of reservoir computing models based on magnetic skyrmions,” *AIP Advances* **8**, 055602 (2018).
- ¹⁹K. M. Song, J.-S. Jeong, B. Pan, X. Zhang, J. Xia, S. Cha, T.-E. Park, K. Kim, S. Finizio, J. Raabe, J. Chang, Y. Zhou, W. Zhao, W. Kang, H. Ju, and S. Woo, “Skyrmion-based artificial synapses for neuromorphic computing,” *Nature Electronics* **3**, 148–155 (2020).
- ²⁰J. Grollier, D. Querlioz, K. Y. Camsari, K. Everschor-Sitte, S. Fukami, and M. D. Stiles, “Neuromorphic spintronics,” *Nature Electronics* **3**, 360–370 (2020).
- ²¹Y. Huang, W. Kang, X. Zhang, Y. Zhou, and W. Zhao, “Magnetic skyrmion-based synaptic devices,” *Nanotechnology* **28**, 08LT02 (2017).
- ²²M. Sharad, C. Augustine, G. Panagopoulos, and K. Roy, “Spin-based neuron model with domain-wall magnets as synapse,” *IEEE Transactions on Nanotechnology* **11**, 843–853 (2012).
- ²³R. Chen, C. Li, Y. Li, J. J. Miles, G. Indiveri, S. Furber, V. F. Pavlidis, and C. Moutafis, “Nanoscale room-temperature multilayer skyrmionic synapse for deep spiking neural networks,” *Phys. Rev. Appl.* **14**, 014096 (2020).
- ²⁴D. Pinna, F. Abreu Araujo, J.-V. Kim, V. Cros, D. Querlioz, P. Bessiere, J. Droulez, and J. Grollier, “Skyrmion gas manipulation for probabilistic computing,” *Phys. Rev. Appl.* **9**, 064018 (2018).
- ²⁵J. Zázvorka, F. Jakobs, D. Heinze, N. Keil, S. Kromin, S. Jaiswal, K. Litzius, G. Jakob, P. Virnau, D. Pinna, K. Everschor-Sitte, L. Rózsa, A. Donges, U. Nowak, and M. Kläui, “Thermal skyrmion diffusion used in a reshuffler device,” *Nature Nanotechnology* **14**, 658–661 (2019).
- ²⁶D. Prychynenko, M. Sitte, K. Litzius, B. Krüger, G. Bourianoff, M. Kläui, J. Sinova, and K. Everschor-Sitte, “Magnetic skyrmion as a nonlinear resistive element: A potential building block for reservoir computing,” *Phys. Rev. Appl.* **9**, 014034 (2018).
- ²⁷K. Raab, M. A. Brems, G. Beneke, T. Dohi, J. Rothörl, F. Kammerbauer, J. H. Mentink, and M. Kläui, “Brownian reservoir computing realized using geometrically confined skyrmion dynamics,” *Nature Communications* **13**, 6982 (2022).
- ²⁸T. Yokouchi, S. Sugimoto, B. Rana, S. Seki, N. Ogawa, Y. Shiomi, S. Kasai, and Y. Otani, “Pattern recognition with neuromorphic computing using magnetic field-induced dynamics of skyrmions,” *Science Advances* **8**, eabq5652 (2023).
- ²⁹Y. Sun, T. Lin, N. Lei, X. Chen, W. Kang, Z. Zhao, D. Wei, C. Chen, S. Pang, L. Hu, L. Yang, E. Dong, L. Zhao, L. Liu, Z. Yuan, A. Ullrich, C. H. Back, J. Zhang, D. Pan, J. Zhao, M. Feng, A. Fert, and W. Zhao, “Experimental demonstration of a skyrmion-enhanced strain-mediated physical reservoir computing system,” *Nature Communications* **14**, 3434 (2023).
- ³⁰C. Frenkel, M. Lefebvre, J.-D. Legat, and D. Bol, “A 0.086-mm² 12.7-pj/sop 64k-synapse 256-neuron online-learning digital spiking neuromorphic processor in 28-nm cmos,” *IEEE Transactions on Biomedical Circuits and Systems* **13**, 145–158 (2019).
- ³¹D. Attwell and S. B. Laughlin, “An energy budget for signaling in the grey matter of the brain,” *Journal of Cerebral Blood Flow & Metabolism* **21**, 1133–1145 (2001).
- ³²J. J. Harris, R. Jolivet, and D. Attwell, “Synaptic energy use and supply,” *Neuron* **75**, 762–777 (2012).
- ³³S. Krishnia, Y. Sassi, F. Ajejas, N. Sebe, N. Reyren, S. Collin, T. Denneulin, A. Kovács, R. E. Dunin-Borkowski, A. Fert, J.-M. George, V. Cros, and H. Jaffrès, “Large interfacial Rashba interaction generating strong spin-orbit torques in atomically thin metallic heterostructures,” *Nano Letters* **23**, 6785–6791 (2023).
- ³⁴W. Jiang, X. Zhang, G. Yu, W. Zhang, X. Wang, M. B. Jungfleisch, J. E. Pearson, X. Cheng, O. Heinonen, K. L. Wang, Y. Zhou, A. Hoffmann, and S. G. E. te Velthuis, “Direct observation of the skyrmion hall effect,” *Nature Physics* **13**, 162–169 (2017).
- ³⁵S. Krishnia, B. Bony, E. Rongione, L. M. Vincente-Arche, S. Collin, A. Fert, J. M. George, N. Reyren, V. Cros, and H. Jaffrès, “Quantifying orbital rashba effect via harmonic hall torque measurements in transition-metalloxide structures,” (2023), arXiv:2309.15987 [cond-mat.mtrl-sci].
- ³⁶M. Schott, A. Bernand-Mantel, L. Ranno, S. Pizzini, J. Vogel, H. Béa, C. Baraduc, S. Auffret, G. Gaudin, and D. Givord, “The skyrmion switch: Turning magnetic skyrmion bubbles on and off with an electric field,” *Nano Letters* **17**, 3006–3012 (2017).
- ³⁷A. Bernand-Mantel, L. Herrera-Diez, L. Ranno, S. Pizzini, J. Vogel, D. Givord, S. Auffret, O. Boulle, I. M. Miron, and G. Gaudin, “Electric-field control of domain wall nucleation and pinning in a metallic ferromagnet,” *Applied Physics Letters* **102**, 122406 (2013).
- ³⁸U. Bauer, L. Yao, A. J. Tan, P. Agrawal, S. Emori, H. L. Tuller, S. van Dijken, and G. S. D. Beach, “Magneto-ionic control of interfacial magnetism,” *Nature Materials* **14**, 174–181 (2015).
- ³⁹L. Herrera Diez, Y. Liu, D. Gilbert, M. Belmeguenai, J. Vogel, S. Pizzini, E. Martinez, A. Lamperti, J. Mohammedi, A. Laborieux, Y. Roussigné, A. Grutter, E. Arenholtz, P. Quarterman, B. Maranville, S. Ono, M. S. E. Hadri, R. Tolley, E. Fullerton, L. Sanchez-Tejerina, A. Stashkevich, S. Chérif, A. Kent, D. Querlioz, J. Langer, B. Ocker, and D. Ravelosona, “Nonvolatile ionic modification of the dzyaloshinskii-moriya interaction,” *Phys. Rev. Appl.* **12**, 034005 (2019).
- ⁴⁰T. Srivastava, M. Schott, R. Juge, V. Křížáková, M. Belmeguenai, Y. Rous-

signé, A. Bernard-Mantel, L. Ranno, S. Pizzini, S.-M. Chérif, A. Stashkevich, S. Auffret, O. Boulle, G. Gaudin, M. Chshiev, C. Baraduc, and H. Béa, “Large-voltage tuning of dzyaloshinskii–moriya interactions: A route toward dynamic control of skyrmion chirality,” *Nano Letters* **18**, 4871–4877 (2018).

⁴¹A. Fassatoui, J. P. n. Garcia, L. Ranno, J. Vogel, A. Bernard-Mantel, H. Béa, S. Pizzini, and S. Pizzini, “Reversible and irreversible voltage manipulation of interfacial magnetic anisotropy in Pt/Co/oxide multilayers,” *Phys. Rev. Appl.* **14**, 064041 (2020).

⁴²T. da Câmara Santa Clara Gomes, T. Bhatnagar-Schöffmann, S. Krishna, Y. Sassi, D. Sanz-Hernández, N. Reyren, M.-B. Martin, F. Brunnett, S. Collin, F. Godel, S. Ono, D. Querlioz, D. Ravelosona, V. Cros, J. Grollier, P. Seneor, and L. H. Diez, “Control of the magnetic anisotropy in multi-repeat pt/co/al heterostructures using magneto-ionic gating,” (2023), arXiv:2310.01623 [cond-mat.mtrl-sci].

⁴³C.-E. Fillion, J. Fischer, R. Kumar, A. Fassatoui, S. Pizzini, L. Ranno, D. Ourdani, M. Belmeguenai, Y. Roussigné, S.-M. Chérif, S. Auffret, I. Jourard, O. Boulle, G. Gaudin, L. Buda-Prejbeanu, C. Baraduc, and H. Béa, “Gate-controlled skyrmion and domain wall chirality,” *Nature Communications* **13**, 5257 (2022).

⁴⁴B. Dai, D. Wu, S. A. Razavi, S. Xu, H. He, Q. Shu, M. Jackson, F. Mahfouzi, H. Huang, Q. Pan, Y. Cheng, T. Qu, T. Wang, L. Tai, K. Wong, N. Kioussis, and K. L. Wang, “Electric field manipulation of spin chirality and skyrmion dynamic,” *Science Advances* **9**, eade6836 (2023).

Acknowledgements This work gets supports from the Horizon2020 Framework Program of the European Commission under FET-Proactive Grant SKYTOP (824123), by the European Research Council ERC under Grant bioSPINspired 682955 and by the French National Research Agency (ANR) with TOPSKY (ANR-17-CE24-0025) and from a France 2030 government grant managed by the French National Research Agency (ANR-22-EXSP-0002 PEPR SPIN CHIREX).

Authors contribution

M.-B.M., P.S., V.C., J.G. and N.R. conceived the project. D.S.-H., Y.S and T.d.C.S.C.G. design the measurement procedure. S.C, Y.S and T.d.C.S.C.G. grew the multilayer films and Ta electrodes. T.d.C.S.C.G. patterned the samples, acquired the MOKE and transport data, treated and analysed the data with support from Y.S, D.S.-H., S.K, M.-B.M., P.S., V.C., J.G. and N.R. T.d.C.S.C.G., V.C., J.G. and N.R. prepared the manuscript. All authors discussed and commented the manuscript.

Competing interests

The authors declare no competing financial interests.